



Photocatalytic degradation of metronidazole and methylene blue by PVA-assisted Bi₂WO₆–CdS nanocomposite film under visible light irradiation

Ranjith Rajendran¹ · Krishnakumar Varadharajan¹ · Venkatesan Jayaraman¹ · Boobas Singaram¹ · Jayaprakash Jeyaram¹

Received: 23 August 2017 / Accepted: 18 December 2017 / Published online: 8 February 2018
© Springer-Verlag GmbH Germany, part of Springer Nature 2018

Abstract

The enhanced photocatalytic performance of nanocomposite is synthesized via the hydrothermal method and characterized using X-ray diffraction (XRD), X-ray photoelectron spectroscopy (XPS), field emission scanning electron microscopy (FESEM), Fourier transform infrared spectroscopy (FT-IR), UV–visible diffuse reflectance spectroscopy (UV–Vis DRS) and photoluminescence spectroscopy (PL). Under visible light irradiation, PVA assisted Bi₂WO₆–CdS nanocomposite film displayed enhanced photocatalytic efficiency and inhibition of photocorrosion as compared with pure CdS, pure Bi₂WO₆ and Bi₂WO₆–CdS composite. The PVA assisted Bi₂WO₆–CdS composite film catalyst showed stable catalytic performance until seven successive runs with 92% of methylene blue (MB) degradation, and easy to recover after degradation of organic pollutant. PVA assisted Bi₂WO₆–CdS nanocomposite film has optimal band edge position for superior photocatalytic degradation. Furthermore, the trapping experiment was carried out using different scavenger for active species. Among the active species, OH[•] are the most responsive species which play a vital role in the degradation of metronidazole and MB.

Keywords Nanocomposite · Optical properties · Trapping experiment · Photocatalytic activity · Methylene blue

Introduction

Dyes play a major role in various branches of dyeing industries such as bleaching, textile, medicine and paper industries (Chauhan et al. 2014; Shanavas et al. 2017). The dye-based industries liberating ~ 10% of non-bio degradable dye wastages with highly colored water, which are deleterious to the environment (Ahmedchekkat et al. 2011; Bazin et al. 2012). The existing dye water leads to interfere with the penetration of light and thus reducing the photosynthesis of aquatic plants which severely annihilate the aquatic ecosystem (Ni et al. 2007). Many organic dyes are toxic and carcinogenic like azo dyes; Congo red, methylene blue and Rhodamine B these may lead to the jeopardizing aquatic organism and also human health (Wong et al. 2004). Generally, the degradation of organic pollutants are mainly classified into three types

such as (1) physical technologies: adsorption, reverse osmosis, ultra-filtration. (2) Chemical process: chlorination, ozonation, precipitation, catalyst-chemical oxidation. (3) Biological process: enzymatic decomposition, biodegradation.

In this regards over the past decades, photocatalytic degradation of organic pollutants and water splitting using nano heterogeneous photocatalyst have immense important due to its feasibility and low cost (Ajmal et al. 2014; Chen and Mao 2007). TiO₂ is one of the most accepted photocatalysts because of biologically and chemically inert (Boobas et al. 2017) and its high photostability, nontoxicity, and low cost, but it has some drawbacks of wide band gap, low quantum yield and only under ultraviolet region (Kudo and Miseki 2009). In case of metal chalcogenides, particularly metal sulfides, have much higher photocatalytic activity (e.g., CdS, ZnS, SnS₂) although metal sulfides are subjected to oxidize by photogenerated holes known as photocorrosion. Among them, various narrow band gap semiconductors, CdS (~ 2.4) can directly absorb visible light at wavelengths ~ 550 nm, which is a good candidate to apply as a photocatalyst. Even though the pure CdS suffered by rapid recombination rate of photogenerated charge carriers and photocorrosion during

✉ Krishnakumar Varadharajan
vkrishna_kumar@yahoo.com

¹ Advanced Materials Laboratory, Department of Physics,
Periyar University, Salem, Tamilnadu 636 011, India

the catalytic action and restricting its potential application. Many researchers focused to overcome the above problem by various technologies (Wang et al. 2016a; Yu et al. 2016). Incorporation of metal sulfides into interlayer and mesoporous materials have a long time efficient for stabilizing the metal sulfides (Shangguan and Yoshida 2002; Shen and Guo 2006). In the midst of various semiconductor photocatalyst, aurivillius family and its layered structure have attractive future and much attention because of hybridized valance band O 2*p* and Bi 6*s* (Tang et al. 2007; Garcia-Perez et al. 2012; Zhu et al. 2013; Dong et al. 2014a). Aurivillius oxide photocatalytic semiconductors ($\text{Bi}_2 \text{A}_{n-1} \text{B}_n \text{O}_{3n+3}$) A = Ca, Sr, Ba, Pb, Na, K and B = Ti, Nb, Ta, Mo, W, Fe (Guo et al. 2013; Zhang et al. 2009; Fu et al. 2005). Bismuth oxyhalide (Chatterjee and Dasgupta 2005; Wang et al. 2011) has the abundant head of the researchers, in the midst of these, Bi_2WO_6 (Saison et al. 2013; Zhuo et al. 2013; Dumrongrojthanath et al. 2013; Saison et al. 2011) has much higher photocatalytic activity and stability in visible and ultraviolet light irradiation and has a wide band gap. However, it also suffered by rapid recombination of photogenerated electrons and holes and unsuitable conduction band edge position (Ren et al. 2015). Meanwhile, among various conjugated polymers, nanocomposites on the polymer substrates or polymer-assisted nanocomposites are attractive to solve the problems concerning the recovery processes during the photocatalytic action. PVA is a hydrophilic polymer which has been explored in a wide range of application including biomaterials and drug delivery system because of biocompatibility and nontoxicity (Jung and Kim 2014; Liu et al. 2015a; Moon et al. 2013; Krishnakumar et al. 2017). Coupling of one or more active components to effectively make heterostructures like $\text{CaWO}_4/\text{Bi}_2\text{WO}_6$ composite, $\text{Bi}_2\text{WO}_6/\text{CeO}_2$ hybrid nanoparticles and $\text{Ag}_2\text{CO}_3/\text{Bi}_2\text{WO}_6$ heterojunction (Guo et al. 2012a, 2014; Bao et al. 2015), are a more powerful method to overcome the demerits of all traditional photocatalyst. In the last few years, making binary nanomaterials using aurivillius oxide semiconductors (Zhang et al. 2016; Liu et al. 2015b) and ternary (CNNS/CdS/rGO), ($\text{CeO}_2/\text{SnO}_2/\text{rGO}$), ($\text{La}_2\text{CuO}_4/\text{CeO}_2/\text{rGO}$) (Zhou et al. 2016; Priyadharsan et al. 2017; Shanavas et al. 2017) plays a vital role in dye degradation. The heterostructure of nanomaterials have much higher efficiency compared to above all, because of interfacial charge transfer between the heterostructure, therefore, it can highly retain the recombination of photogenerated charge carriers.

In this research work, we analyzed the structure and morphology-based many metal chalcogenides, and aurivillius family heterostructure (Kundu et al. 2017; Luo et al. 2016; Kandi et al. 2017; Xiao et al. 2016; He et al. 2011), CdS and Bi_2WO_6 (Tang et al. 2015) have well-matched energy levels and efficient photocatalytic degradation of organic dyes but also had some drawbacks, especially metal sulfides suffered

by photocorrosion. The mixing of photocatalyst nanocomposite with the polymeric substrate is a new way to solve the current problem; recovery of photocatalyst and inhibition of photocorrosion. In our work, as-synthesized Bi_2WO_6 -CdS heterostructures; dispersed into polymer (PVA) matrix. The cost-effective transparent PVA assisted Bi_2WO_6 -CdS nanocomposite film exhibit a recycling stability and ease of recovery in the photodegradation process.

Experimental

Synthesis of CdS nanoparticle

All the chemical reagents and organic targets were of analytical grades and used without further purification. CdS NPs were synthesized by a previously reported hydrothermal route (Cheng et al. 2016), the required molar ratio of $[\text{Na}_2\text{S}\cdot x\text{H}_2\text{O}]$ sodium sulfide solution was added dropwise into the $[\text{CdCl}_2\cdot 2\frac{1}{2}\text{H}_2\text{O}]$ cadmium chloride solution and stirred vigorously for 8 h. The stirred solution was left aging for another 4 h to get the product. Furthermore, it was ultrasonicated with water and transferred into 100 ml Teflon-lined autoclave kept in 24 h at 180 °C. Finally, the yellow color precipitate was washed several times with ethanol and distilled water and the product was dried at 100 °C for 10 h for further characterization.

Synthesis of Bi_2WO_6 -CdS nanocomposite

In the typical synthesis of Bi_2WO_6 -CdS nanocomposite 0.12 g of $[\text{Bi}(\text{NO}_3)_3\cdot 5\text{H}_2\text{O}]$ bismuth nitrate pentahydrate was dissolved in 50 ml of ethylene glycol. On the other hand 0.06 g of $[\text{Na}_2\text{WO}_4\cdot 2\text{H}_2\text{O}]$ sodium tungstate was dissolved in 80 ml deionized water and stirred for 3 h, these two solutions were mixed and stirred until to obtain a homogeneous suspension. Afterwards, the required amount of CdS nanoparticles was dispersed by ultrasonication for 10 min and mixed with this solution. Then the suspension was transferred into the Teflon-lined autoclave kept at 180 °C for 20 h. The product was washed several times using ethanol and distilled water to remove moistures; the finally obtained precipitate is dried at 100 °C for 4 h. The same procedure is repeated for preparation of Bi_2WO_6 nanoparticles without the addition of CdS.

Synthesis of PVA assisted Bi_2WO_6 -CdS nanocomposite film

PVA assisted Bi_2WO_6 -CdS nanocomposite film was prepared via hydrothermal method. The cold soluble polymer was $[-\text{CH}_2\text{CHOH}-]_n$ stirred for 2 h to get a homogenous solution, the prepared Bi_2WO_6 -CdS nanocomposite was ultrasonicated for 30 min and then mixed with the polymer,

continuously stirred for another hour to get a composition. It was transferred into 100 ml Teflon-lined autoclave and gave heat treatment at 180 °C for one hour. Then colloidal solution is poured into silica glass plate and dried to evaporate the solvent.

Characterization methods

Phase structure of the synthesized catalyst was examined by powder X-Ray diffraction using Rigaku X-ray diffractometer Cu-K α radiation ($K = 1.54 \text{ \AA}$) in the 2θ range of 20° – 80° at room temperature. The surface chemical elemental analysis was conducted on an X-ray photoelectron spectroscopy (XPS) (SPECS GmbH spectrometer with Phobios 100MCD Energy analyzer) depth profiling facility. Fourier transform infrared (FT-IR) spectra of all the samples were recorded using a Bruker Tensor 27 spectrophotometer with a resolution of 2 cm^{-1} in the range of 4000 – 400 cm^{-1} at room temperature. Whereas the morphology of the sample was analyzed by field emission scanning electron microscopy [FESEM] with the feature of energy dispersive X-ray diffraction spectrum. Optical properties namely UV–Vis DRS and photoluminescence of the all the prepared catalyst were evaluated by Ocean Optics PX-2 and Perkin Elmer LS-45 fluorescence spectrometer, respectively.

Photodegradation assessment and setup

Methylene blue and metronidazole acted as target substrates for examining the photocatalytic activity of as-synthesized photocatalyst under visible light irradiation. In a typical process $2 \times 2 \text{ cm}^3$ of nano-photocatalyst was dipped (100 ml) in 20 ppm solution of methylene blue. For metronidazole $3 \times 3 \text{ cm}^3$ for 100 ml in 0.1 mg were used, simultaneously the pH value would be monitored. Photodecomposition activity was carried out using 500 W halogen lamp as visible light source and the glassware with double walled for the purpose of circulating water system to maintain a sustained environment of temperature, before the irradiation of visible light. To ensure the formation of adsorption and desorption equilibrium of the organic pollutant with catalyst, the solution was ultrasonicated for 20 min and then stirred for 1 h in dark environment. During the process of decomposition at every 20 min, 6 ml of solution were sampled and centrifuged to remove the catalyst. The photocatalytic efficiency was investigated by the following equations (Mirhoseini and Salabat 2015):

$$\text{Decomposition efficiency (\%)} = \left(\frac{C_0 - C}{C_0} \right) \times 100, \quad (1)$$

where C_0 and C are initial and variable reaction concentration, respectively. In the degradation process, the absorption

intensity for all the catalyst would be A_0 and the significant time interval of the reduced absorption be A , the efficiency was calculated as follows:

$$\text{Efficiency } \eta = \left(\frac{A_0 - A}{A_0} \right) \times 100. \quad (2)$$

To get better understanding of kinetics reaction, the experimental data fitted by a pseudo-first-order model. The equation for calculation is as follows:

$$\ln \left(\frac{C}{C_0} \right) = -K_{\text{app}}t, \quad (3)$$

where C_0 is the initial concentration of dye, C is the concentration at desired time interval K_{app} is the apparent first-order rate constant.

Trapping of active species

The main active species produced in the photodecomposition process of MB and metronidazole confirmed by the trapping agents such as benzoquinone, ethylenediaminetetraacetate, isopropyl alcohol and silver nitrate. They were introduced into to the degradation process to trap superoxide (O_2^-), holes (h^+), hydroxyl (OH^\cdot), and electron (e^-), respectively. All these trapping agents were in the quantity of 5 mmol except BQ which was in 1 mmol to prevent the causes of dye during the reaction. Further, the hydroxyl radicals of all the samples were confirmed by the aid of photoluminescence of terephthalic acid.

Results and discussion

X-ray diffraction analysis

The crystalline structure, appropriate particle size and phase purity of as-synthesized catalysts examined by powder X-ray diffraction pattern. The prepared bare CdS, Bi_2WO_6 , Bi_2WO_6 -CdS and PVA assisted Bi_2WO_6 -CdS nanocomposite film are separately shown in Fig. 1. The sharp peak in the powder X-ray diffraction pattern exposed the well crystalline nature of the prepared sample. Bare Bi_2WO_6 nanoparticle exhibit intense diffraction peaks at 28.16, 32.68, 35.70, 47.07, 51.08, 55.02, 58.54, 68.74, 75.89, 78.30, which corresponds to (113), (006), (115), (206), (224), (313), (226), (400), (139), (406) planes of the russellite (orthorhombic) structure and also exactly matches the JCPDS card No 73-1126. The pure CdS reveals peaks at 24.66, 26.39, 28.30, 36.42, 43.58, 47.64, 51.68, 58.02, 66.74, 69.39, 70.91, 72.35, 75.40, 79.99. Which could be well indexed to the (100), (002), (101), (102), (110), (103), (200), (202), (203), (210), (211), (114), (105), (300) crystal planes of wurtzite (hexagonal) phase [JCPDS card No

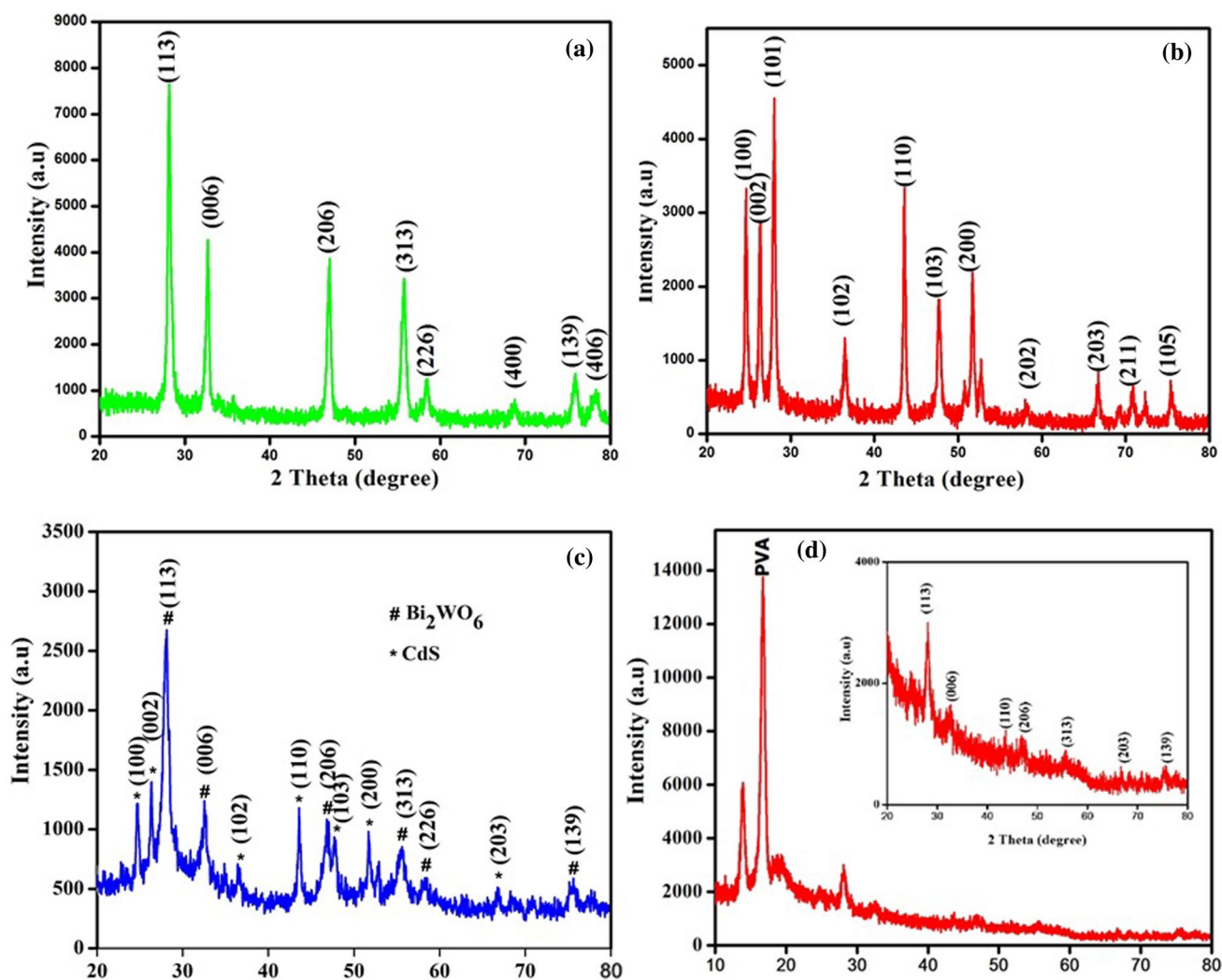


Fig. 1 Powder X-ray diffraction pattern of prepared samples. **a** Bi_2WO_6 , **b** CdS, **c** Bi_2WO_6 -CdS and **d** PVA assisted Bi_2WO_6 -CdS nanocomposite film

06-0314]. In both cases, no additional peaks were found, which shows the absence of other phases or any other impurities. Whereas the XRD pattern of the as-synthesized Bi_2WO_6 -CdS heterostructure, and PVA assisted Bi_2WO_6 -CdS nanocomposites film, possess both Bi_2WO_6 and CdS nanomaterials with less intensity. It could be due to the synergistic effect of the two nanomaterials and additional peaks at 13.86, 16.72 were observed in PVA assisted Bi_2WO_6 -CdS nanocomposite film due to the crystalline and semi-crystalline nature of PVA. The appropriate crystallite size of all the samples calculated using Debye–Scherrer’s equation

$$D = \left[\frac{K\lambda}{\beta \cos \theta} \right], \quad (4)$$

D mean diameter of the crystallite, $K = 0.96$ is constant, λ is wavelength (1.54 \AA), β full width half maximum, θ is diffraction Bragg’s angle.

The structural parameters of the samples like dislocation density (δ), stacking faults (SF), intercrystalline separation (R), are calculated by the following equation (Hemalatha and Rukmani 2016). The values are tabulated in the Table 1.

$$\text{Dislocation density } \delta = \frac{1}{D^2}, \quad (5)$$

$$\text{Stacking fault SF} = \left[\frac{2\pi^2}{45(\tan \theta)^{\frac{1}{2}}} \right] \beta, \quad (6)$$

$$\text{Intercrystalline distance } R = \frac{5\lambda}{8 \sin \theta}. \quad (7)$$

Table 1 Structural parameters of the catalyst

S. no	Nanostructured materials	Average crystalline size (nm)	Dislocation density (10^{14} lines/m)	Inter crystal-lite distance (Å)	Stacking fault (SF)
1	Bi ₂ WO ₆	51.10	4.08	2.96	0.002296
2	CdS	63.92	2.53	3.54	0.001991
3	Bi ₂ WO ₆ -CdS	45.59	7.28	3.48	0.003192
4	PVA (Bi ₂ WO ₆ -CdS)	31.01	10.39	3.96	0.004219

Table 2 Lattice parameters

Catalysts	Phases	<i>a</i> (Å)	<i>b</i> (Å)	<i>c</i> (Å)
CdS	Hexagonal	4.1632	–	6.1478
Bi ₂ WO ₆	Orthorhombic	5.4745	5.2902	16.5127

The lattice parameters calculated using Eqs. (5) and (6) and their values are tabulated in Table 2:

$$\text{Hexagonal } \frac{1}{d^2} = \left[\frac{4}{3}(h^2 + k^2 + hk) + l^2(a/c)^2 \right] \frac{1}{a^2}, \quad (8)$$

$$\text{Orthorhombic } \frac{1}{d^2} = \frac{h^2}{a^2} + \frac{k^2}{b^2} + \frac{l^2}{c^2}. \quad (9)$$

Thus, the hexagonal phases of CdS possess a longer absorption in the visible light region and higher activity compared to cubic phases (Silva et al. 2008; Tian et al. 2012). The bare CdS nanoparticles have to aggregate due to their instabilities; therefore, reducing the aggregation by their heterostructures and doping would enhance the surface area and thus would help to improve the catalytic performance (Kumar and Ojha 2016). Composites show less crystalline nature compared to the pure CdS and Bi₂WO₆ thus it could enhance the crystal surface imperfection like dislocation, stacking faults which turn to increase reaction centers (Zhang et al. 2007). The rate of structural defects could increase the number of chemically reactive sites, and the defects and disorders could change the equilibrium coordination number, that's why chemical reaction would increase further defects tend to lower the bandgap because of the introduction of new band position (Li et al. 2017).

XPS analysis

The oxidation states and surface chemical composition of the nanocomposite film were characterized by X-ray photoelectron spectroscopy (XPS). Typical survey XPS spectrum of Bi₂WO₆-CdS/PVA indicates that Bi, W, Cd, S, C and O elements could all be detected as shown in Fig. 2a. The high-resolution XPS spectra of Bi 4*f*, W 4*f*, Cd 3*d*, S 2*p*,

C 1*s* and O 1*s* is shown in Fig. 2b–g. Figure 2b shows the two bands at 159.15 and 164.16 eV ascribed to Bi 4*f*_{7/2} and Bi 4*f*_{5/2}, respectively, which can be attributed to Bi³⁺ in the crystal structure. The peak at 36.2 and 37.6 eV as shown in Fig. 2c, corresponding to W 4*f*_{7/2} and W 4*f*_{5/2}, respectively, can assign to be a W⁶⁺ oxidation state of Bi₂WO₆-CdS/PVA (Zhang et al. 2006). Figure 2d represents the binding energies of 405.28 and 412.60 eV corresponds to the Cd 3*d*_{5/2} and Cd 3*d*_{3/2} respectively (Li et al. 2013). The S 2*p* spectrum was divided into two different peaks is shown in Fig. 2e. The peak at 161.15 eV could be a credit to the S²⁻ anion, and the other one at 167.12 eV could be assigned to the oxidized SO₄²⁻ form (Bandyopadhyay et al. 1997). From Fig. 2f, it was observed that the peaks with binding energies of 284.2 and 287.65 could be assigned to the C 1*s* spectra of C–C and C–O, respectively. The C–C bond bond confirm the main chain of PVA (Wei et al. 2011). Furthermore, Fig. 2g show that two peaks fitted the O 1*s* spectrum. The peak at 530.35 eV can be due to the metal oxides, the broad peak at 533.04 eV indicates the binding energy of C–OH bond in PVA (Gu et al. 2012). Based on these observations and analyses the results exhibit that the formation of Bi₂WO₆-CdS/PVA composite occurs, which is in better agreement with the results of the EDX and XRD analysis.

FT-IR analysis

The chemical state of as-synthesized Bi₂WO₆, CdS, Bi₂WO₆-CdS and PVA assisted Bi₂WO₆-CdS nanocomposite film explored via FT-IR spectroscopy and their spectrograms are shown in Fig. 3. The spectrum reveals the band absorption peak at 3000–3600 cm⁻¹ in bare nanoparticles is assigned to the OH stretching vibration of a physically observed water molecule. In Bi₂WO₆ several characteristic peaks were observed at wavenumbers 1395, 725, 583 cm⁻¹ are due to the W–O–W bridging, W–O stretching, Bi–O stretching vibration, respectively (Liu et al. 2015c; Wei et al. 2014; Guo et al. 2012b). In the case of CdS, Cd–S stretching vibration occurred below 700 cm⁻¹. Meanwhile, PVA assisted Bi₂WO₆-CdS nanocomposite film shows vibrations at 3000–3109 cm⁻¹ are due to the O–H stretching vibration hydroxyl groups due

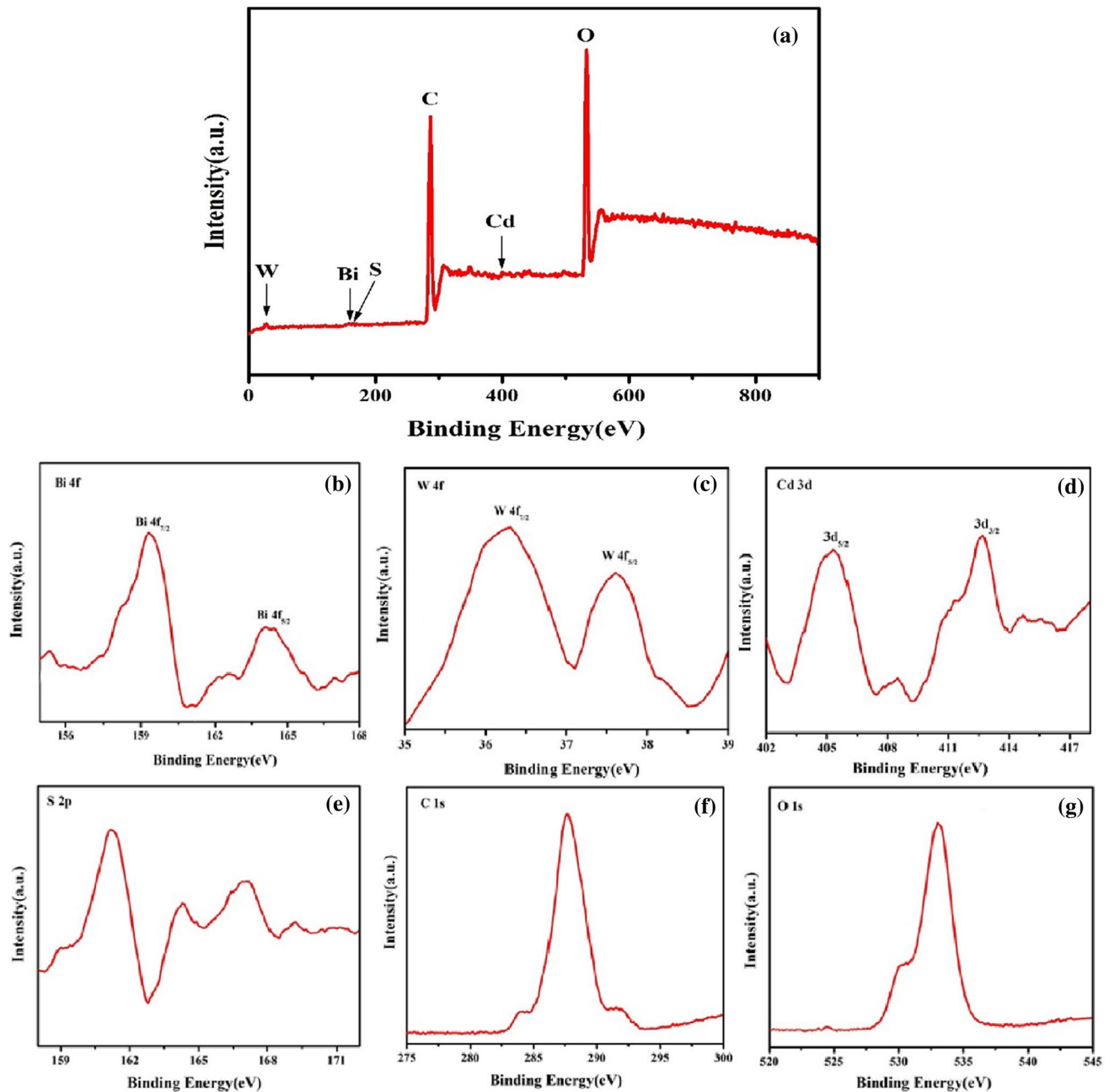


Fig. 2 XPS spectra of PVA assisted Bi₂WO₆-CdS nanocomposite film. **a** Survey spectrum; **b** Bi 4f; **c** W 4f; **d** Cd 3d; **e** S 2p; **f** C 1s; **g** O 1s

to polymeric or water molecules, and then CH, C=O, C=C, and C-C stretching, rocking vibrations are assigned at 2970, 1746, 1605, 1525 and 900 cm⁻¹, respectively (Krishnakumar and Shanmugam 2012; Chen 2002; Rao et al. 2015; Mallakpour and Vahabi 2015). In PVA assisted Bi₂WO₆-CdS nanocomposite film, the content of nanoparticle loading is very low, therefore, the interaction of nano heterostructures with nanostructured polymer was unpredictable from the FT-IR spectrum.

Morphology analysis

The surface morphology of all prepared samples was characterized by FESEM and their micrographs are shown in Fig. 4. It was observed that the bismuth tungstate shows spheroid structure. CdS show loosely agglomerated well-defined spherical shape with the high surface area, meanwhile, in the case of Bi₂WO₆-CdS nanocomposite CdS nanospheres were sprinkled on the core Bi₂WO₆ structure.

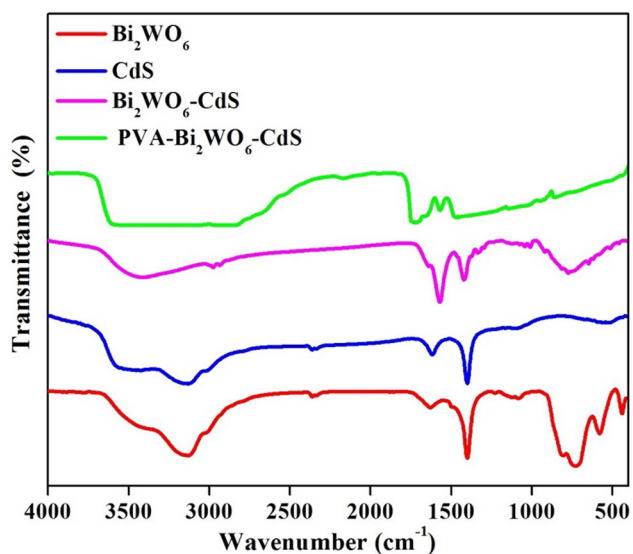


Fig. 3 FT-IR spectrum of the prepared samples

The CdS nanosphere agglomeration get suppressed when it is adhered to the surface of Bi_2WO_6 and their particle size could enhance by deposition of CdS. In the case of PVA assisted Bi_2WO_6 -CdS nanocomposite film, the dark spot shows a shapeless surface passivated structure which is attributed to the crystalline nature of polymer in nanoscale, the bright spot indicates the surface modified agglomerated Bi_2WO_6 -CdS nano-heterostructures. This type of morphology might enhance the photocatalytic degradation performance.

EDX analysis

The representative EDX spectra of synthesized samples examined by the integrated feature of FESEM, and their graphs are shown in Fig. 5. In Bi_2WO_6 the Bi, W, O elements were confirmed and their wt% are 48.15, 35.09, 16.76, respectively. The established CdS spectra show Cd, S element with 76.10, 23.10 wt% correspondingly. Whereas the Bi_2WO_6 -CdS shows the presence of above-mentioned all elements with slight changes in wt% (Cd, Bi, W, O, S

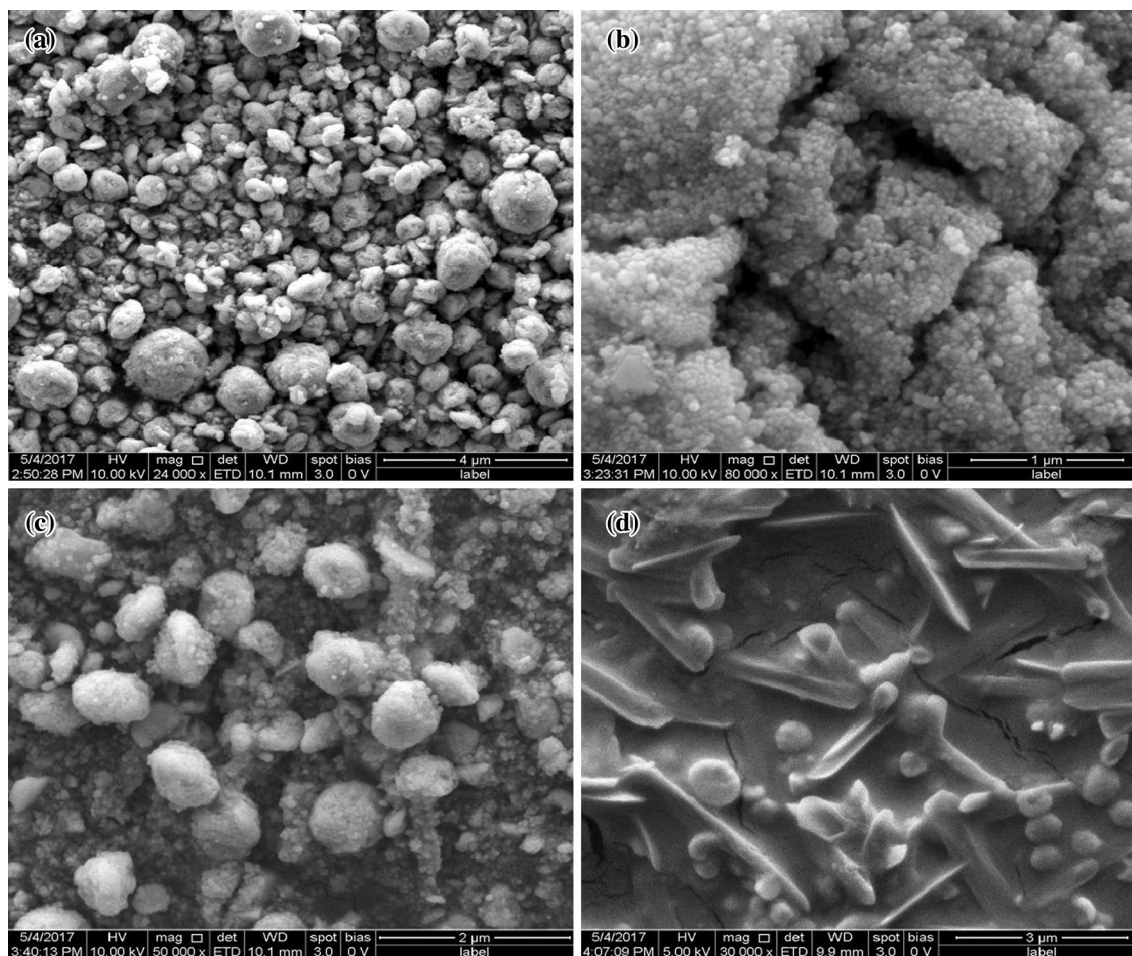


Fig. 4 The FESEM images of a Bi_2WO_6 , b CdS, c Bi_2WO_6 -CdS and d PVA assisted Bi_2WO_6 -CdS film

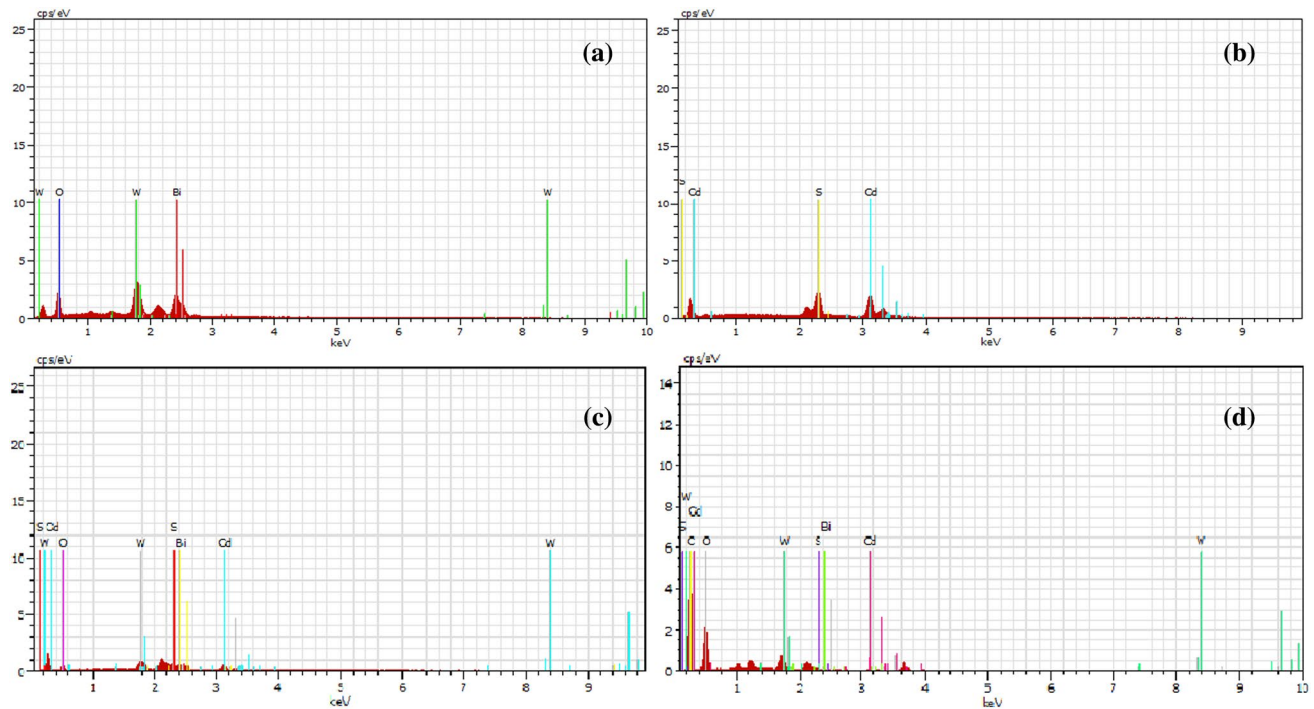


Fig. 5 EDX spectrum of **a** Bi_2WO_6 , **b** CdS, **c** Bi_2WO_6 -CdS and **d** PVA assisted Bi_2WO_6 -CdS nanocomposite film

with 29.78, 26.98, 25.55, 9.08, 8.60 wt% singly). But PVA assisted Bi_2WO_6 -CdS nanocomposite film confirms the presence of H, C, O, Cd, Bi, W, S elements with 51.73, 23.57, 15.97, 1.65, 0.26, 6.15, 0.69 wt%, respectively. No other impurities are found in all the samples.

UV-Vis diffuse reflectance spectra

All the prepared photocatalysts subjected to optical characterization of UV-Vis DRS techniques using Ocean Optics PX-2 spectrophotometer, and the results are shown in Fig. 6. The Bi_2WO_6 nanoparticle exhibited the strong absorption edge ultraviolet and visible region approximately 420 nm is owing to the band gap photoexcitation of Bi_2WO_6 . On the other hand, CdS exhibit the intensive absorption edge around 600 nm due to its response to visible light. When adding CdS to Bi_2WO_6 the absorption edge shows blue shifts 575 nm and it could gather few number of photons compared to bare Bi_2WO_6 and CdS (Zou et al. 2016). Then the PVA assisted Bi_2WO_6 -CdS composite film also exhibited absorption edge in visible region 560 nm. This blue shift of absorption indicates that the composites exhibit quantum confinement effect (Jing and Guo 2007). From above obtained results PVA assisted Bi_2WO_6 -CdS nanocomposite film has higher absorption maximum in the visible region. The band gaps of all the samples were calculated with the help of tauc plot and shown in inset Fig. 6 using the following equation (Zheng and Liu 2007)

$$(\alpha h\nu)^2 = A(h\nu - E_g), \quad (10)$$

α is the absorption coefficient, h is the plank constant, ν is the frequency of light, E_g is the band gap, A is the proportionality constant, respectively, $n = (1, 4)$ depend on the type of optical transition whether direct or indirect. Therefore, plotting between $(\alpha h\nu)^2$ and $(h\nu)$ by extrapolating the linear portion of the curve to zero absorption coefficient. The band gap of pure Bi_2WO_6 , CdS, Bi_2WO_6 -CdS and PVA assisted Bi_2WO_6 -CdS nanocomposite film calculated, and their values are given by 3.32, 2.16, 2.25 and 2.41 eV, respectively. The PVA assisted Bi_2WO_6 -CdS nanocomposites film show low band gap compared to that of Bi_2WO_6 materials, because of changes in optical properties suffered by the interaction between the pure CdS and Bi_2WO_6 nanomaterials (Guo et al. 2016). Although the band gap of PVA assisted Bi_2WO_6 -CdS nanocomposites film, due to the intermediate transaction of electrons in between the composite materials the recombination rate will be declined and the observed result is further confirmed through PL study. These results illustrate that the PVA assisted Bi_2WO_6 -CdS nanocomposite film can be excited in visible light region due to the deposition of CdS nanoparticles on its surface.

Photoluminescence spectroscopy

Photoluminescence spectroscopy is used to assess the recombination efficiency of photogenerated electrons and

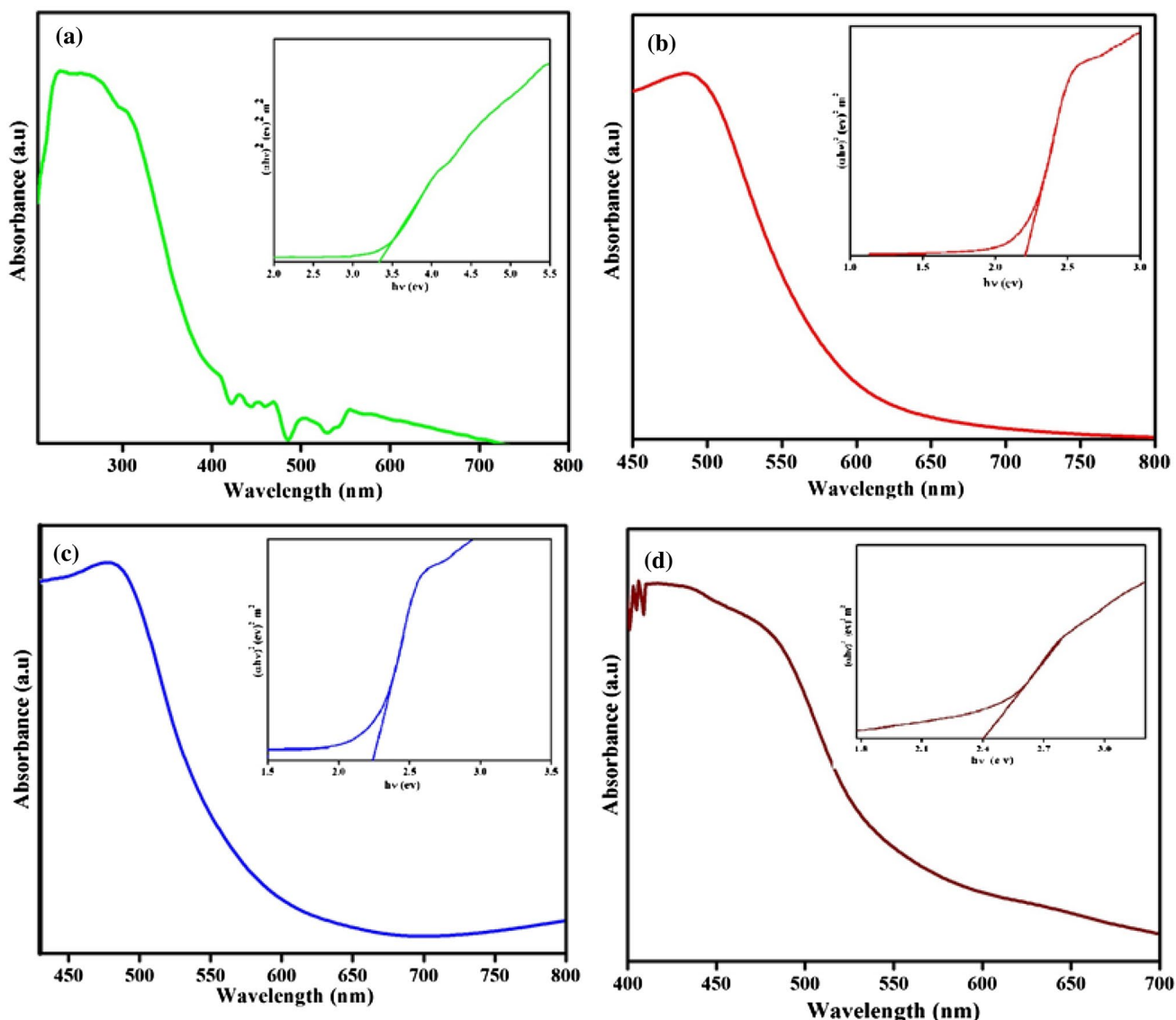


Fig. 6 UV-Vis DRS spectra of **a** Bi_2WO_6 , **b** CdS, **c** Bi_2WO_6 -CdS and **d** PVA assisted Bi_2WO_6 -CdS nanocomposite film

holes in photocatalytic reaction. Photoluminescence properties of all the products are shown in Fig. 7. The more intense peak assigned to CdS and thus more emission occurs due to a large amount of recombination of photogenerated charge carriers. The Bi_2WO_6 and PVA could reduce the photoemission, and the composite often indicates a drastic decrease in its intensity and confirmed the sensible suppression and recombination of electron and hole which improved photocatalytic activity. PVA/ Bi_2WO_6 -CdS has narrow optical band gap than Bi_2WO_6 , this could give highly harvesting photons from UV-Vis light, and it could retain the recombination of generated charge carriers. The PL intensity of PVA assisted nanocomposite film shows less intensity compared to all other prepared photocatalyst, thus result from most of the surface states are passivated by making the availability

of the electron for catalytic action (Wang et al. 2016b). The weaker PL intensity is, the higher separation efficiency of photoinduced charge (electron-hole separation), so that higher photocatalytic degradation behavior was preferred. Thus, the result indicates that compared with pure CdS and Bi_2WO_6 samples, the photocatalytic efficiency of PVA/ Bi_2WO_6 -CdS photocatalyst may be greatly improved.

Photocatalytic degradation of metronidazole

Drugs occupy an important place in the water pollution due to the availability of many healthcare products such as antibiotics, analgesics, anti-inflammatories and hypnotics, and high consumption rate of a human being and veterinary medication (Kansal et al. 2014). The drugs occupy the aquatic

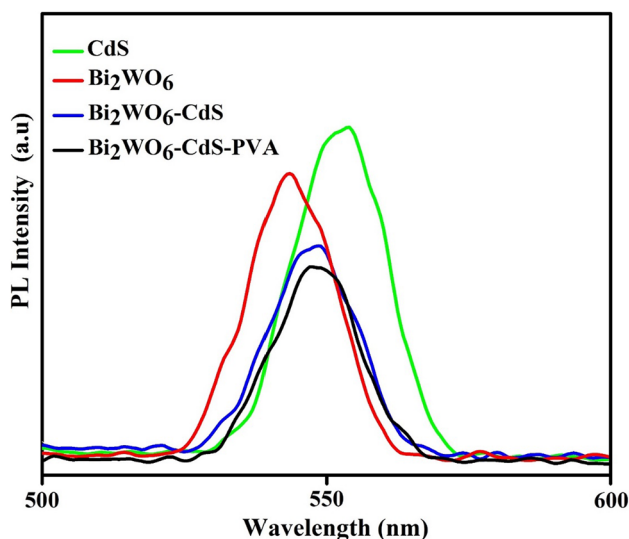


Fig. 7 Photoluminescence spectra of the samples

environment from various ways such as pharmaceuticals, industrial effluents and domestic effluents, the disposal of rude discarding of extra drugs in households, medicinal care, and healing treatment of livestock (Farzadkia et al. 2014). High concentration of antibiotics can involve serious risk for the human being and natural system because high solubility causes them, long-term presence, more toxic, cancerogenic, less adsorption, non-biodegradability nature. The effluent of wastewater from pharmaceuticals industries must be treated adequately before entry into natural water streams, to remove the contaminant caused by antibiotics. In over the past decades antibiotic effluents from industries act as a target pollutants to degrade using photocatalyst such

as quinoline content and levofloxacin (Kansal et al. 2014), amoxicillin, glycopeptide, macrolide, sulphonamide (Kummerer 2009), tetracycline (Safari et al. 2015; Zhao et al. 2013), sulfamethoxazole (Abellan et al. 2009; Abellan et al. 2007), chloramphenicol (Chatzitakis et al. 2008) and metronidazole (Farzadkia et al. 2014). Among them metronidazole has been studied by many researchers, metronidazole antibiotics (2-methyl-5-nitro-imidazole-1-ethanol) was a derivative of nitroimidazole, which was widely used in the treatment of infectious diseases like anaerobic bacteria, protozoans, Bacteroides. Continuous and increasing the content of metronidazole is more carcinogenic and mutagenic, researchers have been paid mandatory to remove this type of contaminants completely before they are discharged from industries (Farzadkia et al. 2014; Liu et al. 2013; Dong et al. 2014b) here by all the problems aforementioned we choose metronidazole as a target organic contaminants.

The photocatalytic activities of pure CdS, Bi_2WO_6 , binary Bi_2WO_6 -CdS and PVA- Bi_2WO_6 -CdS nanocomposite were evaluated by the metronidazole shown in Fig. 8a. From the result, PVA- Bi_2WO_6 -CdS nanocomposite shows enhanced photocatalytic efficiency when compared to other binary composites such as Bi_2WO_6 -CdS and parent photocatalysts like Bi_2WO_6 and CdS. The parent photocatalyst shows the limited amount of catalytic efficiency, but after coupling PVA with of CdS- Bi_2WO_6 , the photocatalytic degradation of metronidazole significantly enhanced, achieving almost 70% after the irradiation of visible light for 100 min. Due to the composition of CdS- Bi_2WO_6 with PVA can serve as charge traps thus could retarding electron-hole combination rate and thereafter enhancing the interfacial charge transfer for metronidazole degradation. In addition to this connection, PVA

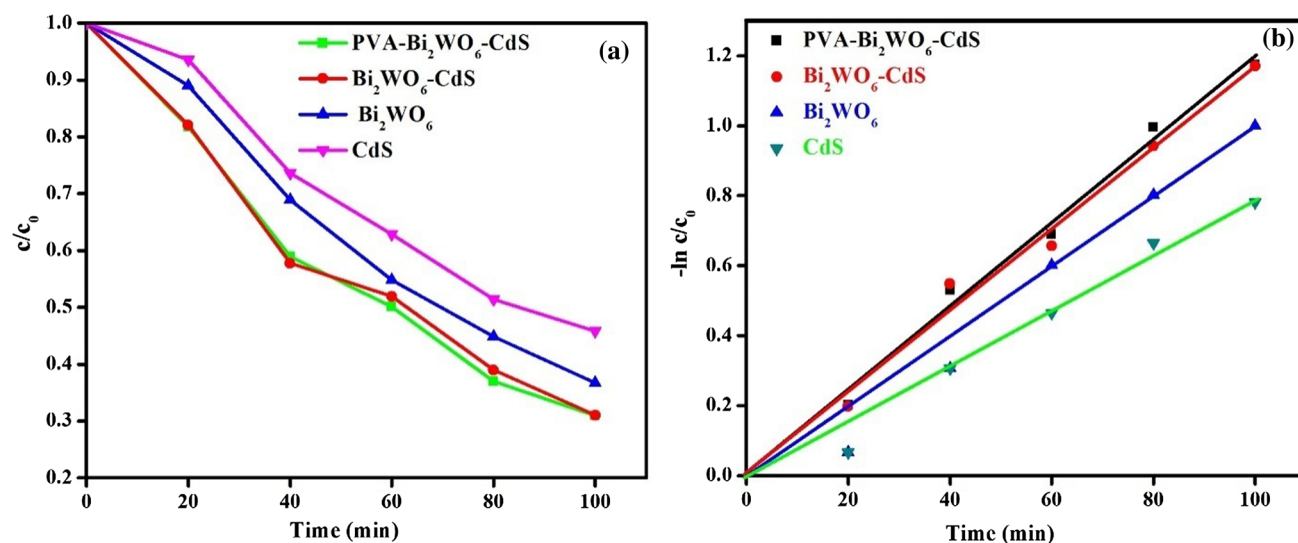


Fig. 8 Photocatalytic degradation of metronidazole **a** efficiency under the presence of different catalyst, **b** their first-order pseudo kinetics

coupled with binary Bi_2WO_6 -CdS composite the photocorrosion phenomenon would be minimized, so that the durability and photostability increased. To understand the photocatalytic activity of pure CdS, Bi_2WO_6 , binary Bi_2WO_6 -CdS, and PVA- Bi_2WO_6 -CdS nanocomposite can be described by pseudo-first-order kinetics, in Fig. 8b shows a linear relationship between $\ln(C_0/C)$ and reaction time, indicating that the photodegradation of metronidazole follows first-order kinetics. The calculated values of K_{app} or K were given by 0.0120, 0.0110, 0.0090 and 0.0070 for PVA assisted Bi_2WO_6 -CdS, Bi_2WO_6 -CdS, Bi_2WO_6 , and CdS, respectively. Indeed thus from the values of K it is clear that the PVA assisted Bi_2WO_6 -CdS nanocomposite film shows highest photocatalytic activity. A nanocomposite film possesses more activity 1.7142, 1.333 and 1.0909 times higher than CdS, Bi_2WO_6 and Bi_2WO_6 -CdS, respectively; this is due to highly suppressed photogenerated carriers. Furthermore, UV-visible spectra confirmed the enhanced photocatalytic degradation efficiency of PVA- Bi_2WO_6 -CdS nanocomposite film an antibiotic solution of metronidazole. The absorption spectrum of efficient PVA- Bi_2WO_6 -CdS nanocomposite film are shown in Fig. 9. The absorption spectra of metronidazole show the characteristic peak (absorption maximum) at approximately λ_{max} 320 nm. The photocatalytic degradation of metronidazole observed for every 20 min time interval at constant irradiation of UV-visible light. From the observation of absorption spectrum, drastically decrease the absorption maximum, it strongly indicates decomposition nature of metronidazole solution. So that, PVA- Bi_2WO_6 -CdS nanocomposite film has an excellent photocatalytic activity compared to the CdS, Bi_2WO_6 , Bi_2WO_6 -CdS catalyst.

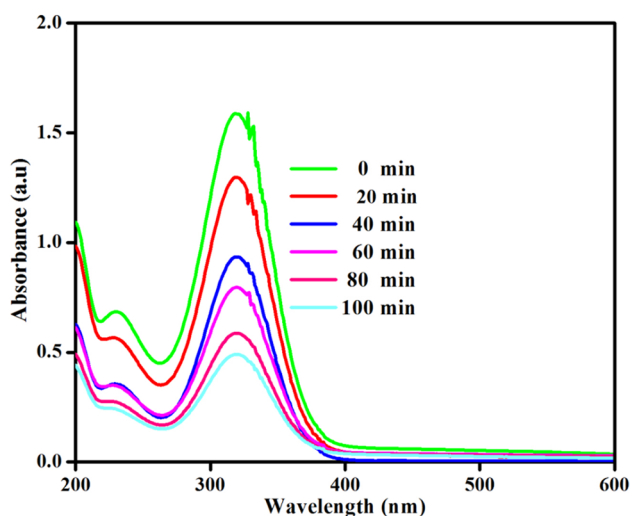


Fig. 9 Photocatalytic degradation of metronidazole with PVA assisted Bi_2WO_6 -CdS nanocomposite film

Photocatalytic degradation MB

On basis of all aforementioned photocatalytic performance of catalysts like individuals and their composites were evaluated by the degradation of MB exposed to visible light irradiation, before that the adsorption test was carried. There was no degradation observed in the absence of catalysts, which was obviously the stability of MB under self-photolysis. For comparison purpose, the photocatalytic activity of bare CdS, Bi_2WO_6 , binary Bi_2WO_6 -CdS and PVA- Bi_2WO_6 -CdS nanocomposite against MB is shown in Fig. 10. Where net visible, light irradiating time was to be 100 min, and the absorption intensity was measured peak position at 664 nm, during the reaction absorption intensity was monitored for every 20 min. The results show that the bare CdS and Bi_2WO_6 shows low activity against degradation MB for 100 min that was 72 and 86%, respectively. Meanwhile, PVA assisted Bi_2WO_6 -CdS nanocomposite film gave much higher efficiency (92%) compared to binary Bi_2WO_6 -CdS and neat catalysts. Further, the higher degradation efficiency of PVA assisted Bi_2WO_6 -CdS nanocomposite film, confirmed in Fig. 11a. Clearly, the photocatalytic activity of binary Bi_2WO_6 /CdS composites boosts with the addition of CdS when compared to pure Bi_2WO_6 . The difference in photocatalytic activity may relate to visible light absorption properties, the separation efficiency of photogenerated electrons and holes and efficient charge transfer. CdS are normally charge carriers, both electrons and holes quickly recombine and only a fraction are contributed in the photocatalytic reaction process causing low reactivity and also Bi_2WO_6 nanoparticles exhibit the lowest photocatalytic activity, which may result from its large band gap. According to the band gap calculation above, the band gap of Bi_2WO_6 is 3.32 eV, indicating poor absorbance of light in the visible region. The degradation rate of MB was analyzed by the pseudo-first-order kinetic process over CdS, Bi_2WO_6 , Bi_2WO_6 -CdS and PVA assisted Bi_2WO_6 -CdS nanocomposite film and the results shown in Fig. 11b. Photoreaction kinetics rate of the CdS, Bi_2WO_6 , Bi_2WO_6 -CdS and PVA assisted Bi_2WO_6 -CdS nanocomposite film were 0.012, 0.015, 0.022 and 0.024, respectively. The PVA assisted Bi_2WO_6 -CdS nanocomposite film were 1.0909 times higher than Bi_2WO_6 -CdS heterostructures and 1.6, 2 times higher than bare Bi_2WO_6 , CdS.

Proposed possible mechanism

Based on the above discussion, the possible photocatalytic mechanism for PVA assisted Bi_2WO_6 -CdS nanocomposite film was proposed and shown in Fig. 12. Under the visible light, irradiation of CdS was excited and produced the photogenerated charge carriers. When the excited electron in the CB of CdS where transferred into the CB of Bi_2WO_6 .

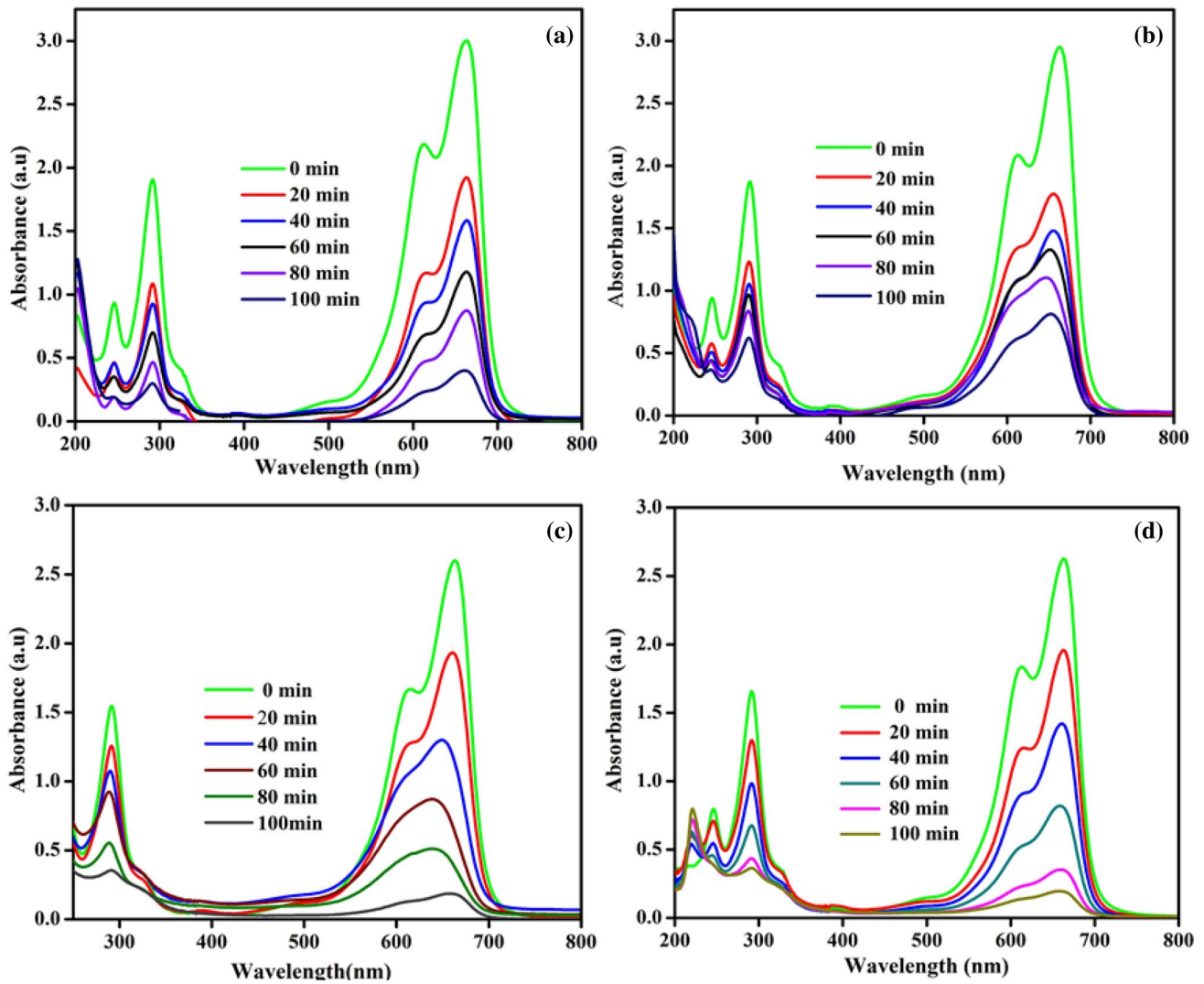


Fig. 10 Photocatalytic degradation of MB. **a** Bi_2WO_6 , **b** CdS, **c** $\text{Bi}_2\text{WO}_6\text{-CdS}$, **d** PVA assisted $\text{Bi}_2\text{WO}_6\text{-CdS}$ nanocomposite film

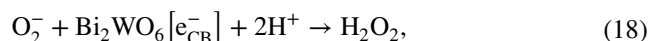
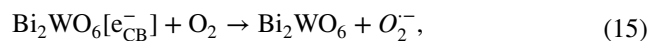
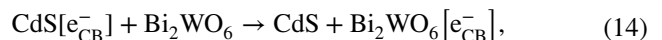
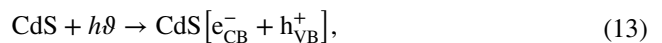
While excited holes in the VB of Bi_2WO_6 shifted to the CB of CdS. There was a suppression of photogenerated charge carriers and free transfer of separated electron and holes towards the surface for the availability of carriers for oxidation and reduction. The conduction band (CB) and valence band (VB) edges were determined using the following equations:

$$E_{\text{CB}} = \chi - E_e - 0.5E_g, \quad (11)$$

$$E_{\text{CB}} = E_{\text{VB}} - E_g, \quad (12)$$

χ is the absolute electronegativity of semiconductor which is geometric mean of constitute of atoms E_e is the energy free electrons on the hydrogen scale (~ 4.5 eV), the absolute electronegativity was 5.19 for CdS (Zou et al. 2016) and 6.36 for Bi_2WO_6 (Wang et al. 2017) and the calculated band

edge positions are tabulated in Table 3. The degradation of model pollutants such as metronidazole and MB described in the following reaction



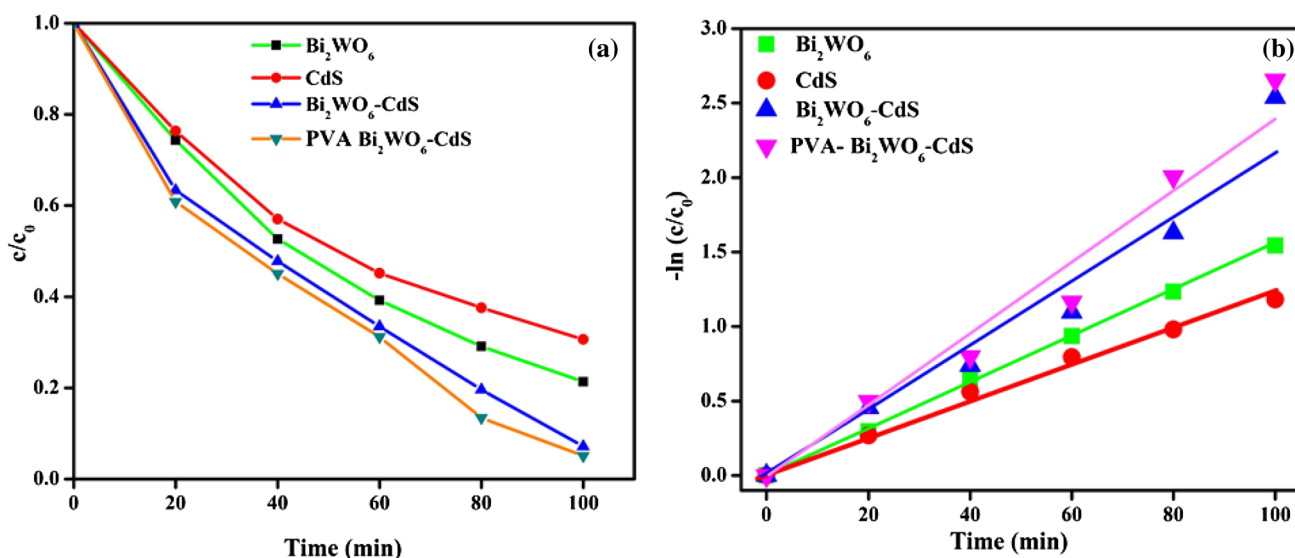


Fig. 11 Photocatalytic degradation of MB. a Efficiency of all the prepared photocatalyst. b First-order pseudo kinetic study

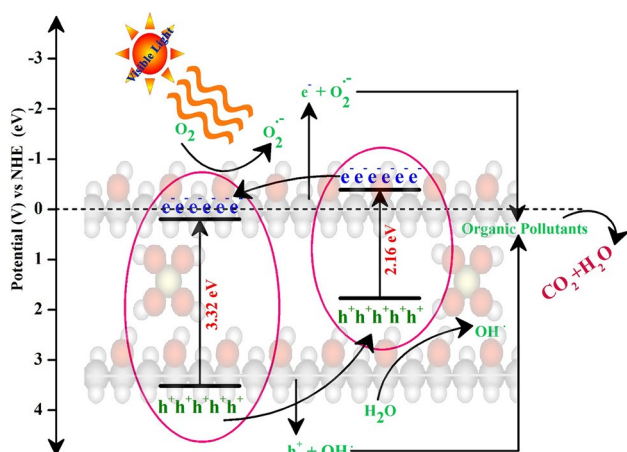


Fig. 12 Schematic illustration of band edge position and interfacial charge transfer of the PVA assisted $\text{Bi}_2\text{WO}_6\text{-CdS}$ nanocomposite film

Table 3 Calculation of band edge position

Catalyst	E_{CB} (eV)	E_{VB} (eV)	E_g (eV)
Bi_2WO_6	0.20	3.52	3.32
CdS	-0.39	1.77	2.16



From the mechanism pathway, PVA assisted $\text{Bi}_2\text{WO}_6\text{-CdS}$ nanocomposite film produced a large amount of highly reactive species like OH^\cdot than that of less reactive species such as O_2^- radical. So that photocatalytic activity drastically increases PVA assisted $\text{Bi}_2\text{WO}_6\text{-CdS}$ nanocomposite film, because of the large amount and highly reactive OH^\cdot radical production. Meanwhile, the contribution of PVA on $\text{Bi}_2\text{WO}_6\text{-CdS}$ composite immense fashion, due to the special character of minimizing photocorrosion and photostability.

Trapping of active species

The active species trapping measurements is significant to examine the active species in the photocatalytic process for a better understanding of photocatalytic mechanism. In degradation of dyes, several active radical species such as hole (h^+), hydroxyl radicals (OH^\cdot), superoxide anion radical (O_2^-) and electron (e^-) plays major contribution. The active species trapping experiments toward PVA assisted $\text{Bi}_2\text{WO}_6\text{-CdS}$ nanocomposite film are carried out, and the results are shown in Fig. 13. Primarily, all the four established species with a photogenerated hole (h^+), hydroxyl (OH^\cdot) radical superoxide anion radical (O_2^-) and electron (e^-) are active during the photocatalytic process. Almost adverse change exist in the presence of IPA, implying that OH^\cdot radicals had a large effect on the degradation process under visible light illumination. In contrast, an apparent reduction was observed upon the addition of BQ compared to the case IPA, and a radical inhibition was superficial after

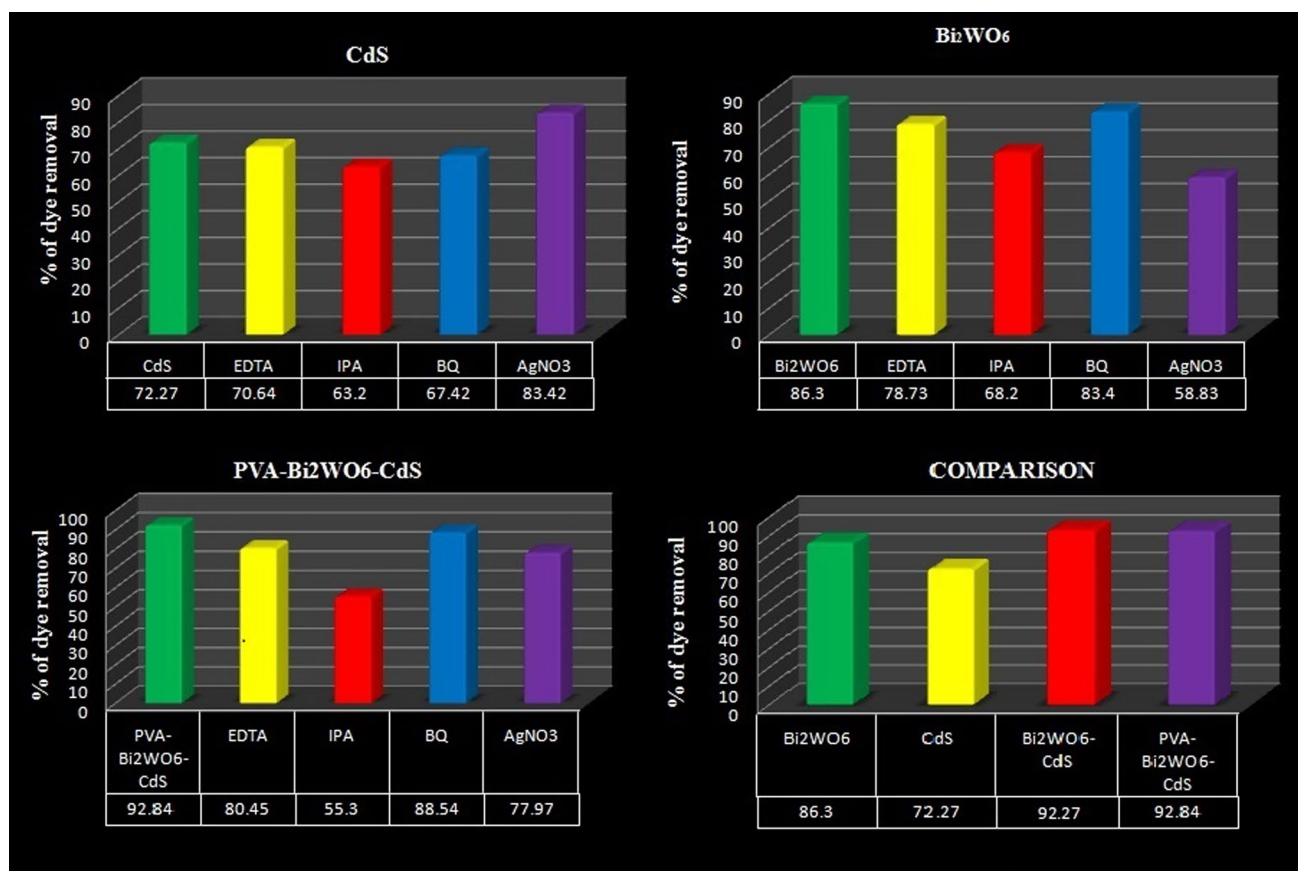


Fig. 13 Trapping of active species

the addition of EDTA, suggesting that O_2^- radicals and/or h^+ were the main reactive species of the PVA assisted $\text{Bi}_2\text{WO}_6\text{-CdS}$ nanocomposite film and played significant roles in the photocatalytic process under visible light illumination. Moreover, the photocatalytic degradation rate of model pollutants solution using EDTA and AgNO_3 was lower than that using IPA, revealing that OH^\cdot played the most significant role in the photocatalytic process under visible light illumination.

Detection experiment for hydroxyl radicals

In general, the hydroxyl radicals (OH^\cdot), a highly reactive species with strong oxidation ability, were considered mainly responsible for the degeneration of pollutant molecules in the photocatalytic reaction. The concentration of hydroxyl radicals was detected during the reaction with the help of terephthalic acid by photoluminescence spectra. The taken terephthalic acid is reacting with OH^\cdot radicals when

produced at the reaction and convert into a highly luminescent 2-hydroxy terephthalic acid. The intensity of PL spectra is directly proportional to the formation of 2-hydroxy terephthalic acid in the reaction of terephthalic acid with OH^\cdot in photocatalysis system (Sarkar et al. 2016; Zeng et al. 2017). The UV-Vis absorbance and detection of OH^\cdot radicals for PVA assisted $\text{Bi}_2\text{WO}_6\text{-CdS}$ nanocomposite film using PL spectra is shown in Fig. 14. The UV-Vis absorbance gives a strong absorbance at 233 nm, then PL spectra of the produced 2-hydroxy terephthalic acid were monitored two peaks at approximately 345, 420 nm, respectively. PVA $\text{Bi}_2\text{WO}_6\text{-CdS}$ show more PL intensity, due to producing a significant amount of OH^\cdot radicals. The same experiment was carried out with the bare photocatalyst like CdS and Bi_2WO_6 . From the OH^\cdot radical detection processes, the PL intensity of Bi_2WO_6 and CdS has low when compared with PVA assisted $\text{Bi}_2\text{WO}_6\text{-CdS}$ nanocomposite film. Figure 14b–d shows the PL intensity of formation of 2-hydroxy terephthalic acid in presence of Bi_2WO_6 and CdS.

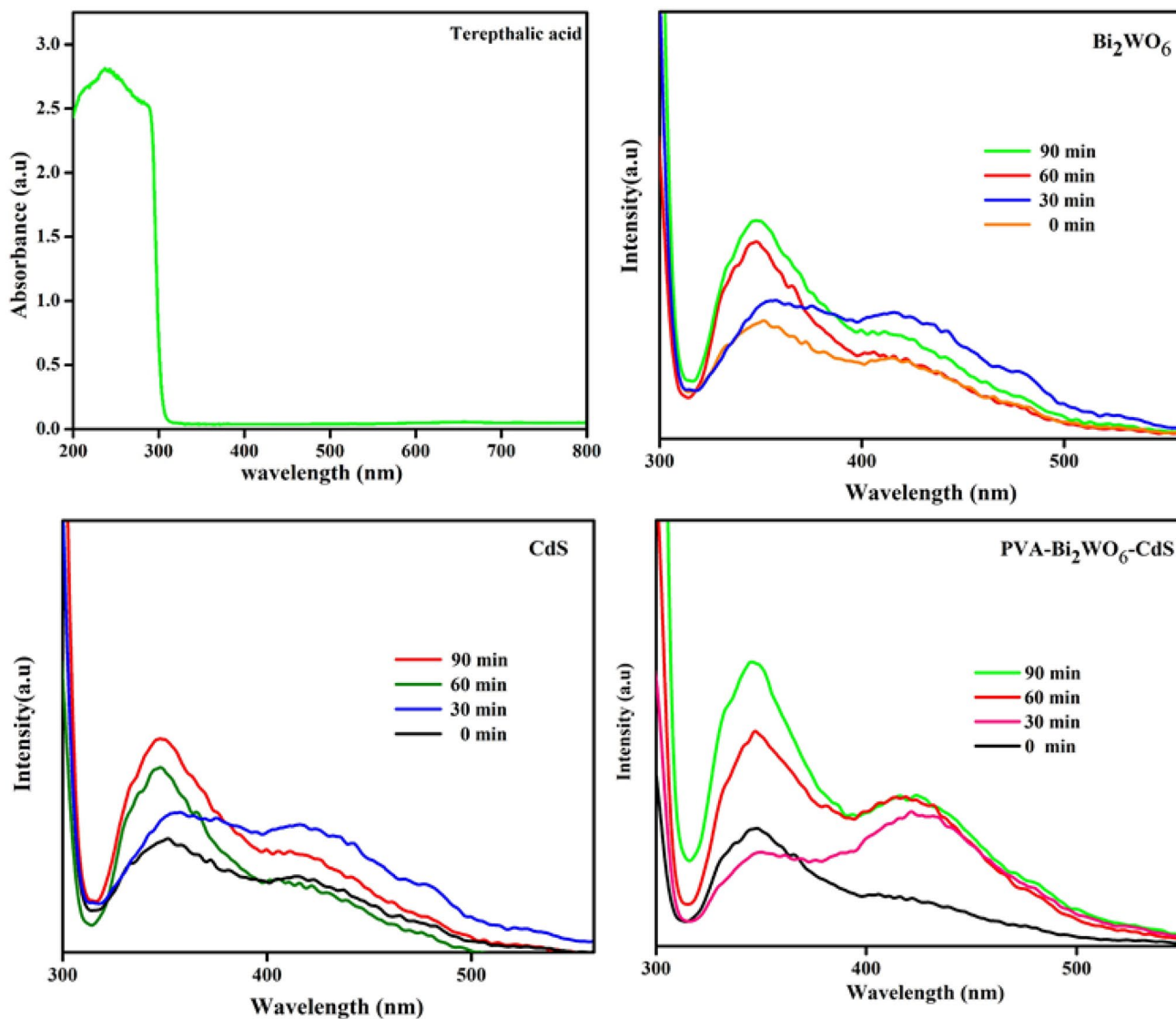


Fig. 14 Detection of hydroxyl radical using terephthalic acid as probe molecule

Recycling exploration

In the practical applications of photocatalysis, the reusability, as well as stability, had a more important which when act as a catalyst. The recycling experiment was carried out for the prepared PVA assisted Bi₂WO₆-CdS nanocomposite film under an aforementioned same reaction condition; here the nanocomposite film was separated after the degradation of organic pollutant. Then it was dipped into another 100 ml of MB solution. The efficiency of Photodegradation of MB for every cycle is shown in Fig. 15. There was no obvious loss until seven cycles after that obviously minimum decline in photocatalytic activity.

Conclusion

In summary, PVA assisted Bi₂WO₆-CdS nanocomposite film photocatalyst was successfully synthesized through hydrothermal method. The PVA assisted Bi₂WO₆-CdS nanocomposite film showed better photocatalytic activity and photostability than that of pure CdS and pure Bi₂WO₆ toward the degradation of both MB and metronidazole under visible-light irradiation. The attractive nature of PVA assisted Bi₂WO₆-CdS nanocomposite film was easy to recover from the degradation system after the photocatalytic degradation performance. The PVA play a vital role in the retired recombination rate of photon-generated carriers,

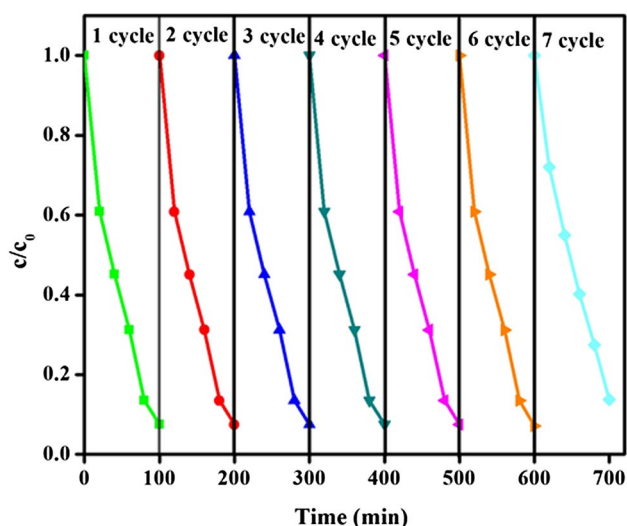


Fig. 15 Recycling exploration of PVA assisted Bi_2WO_6 -CdS nanocomposite film

accordingly promote the activity and stability of the catalyst. This work will deliver a new way for efficient photocatalyst and reduced photocorrosion.

Acknowledgements The authors thank Department of Physics, Indian Institute of Science, Bangalore for XPS Analysis. One of the authors Ranjith Rajendran acknowledges Periyar University for providing financial support in the form of University Research Fellowship (URF) grant.

References

- Abellan MN, Bayarri B, Gimenez J, Costa J (2007) Photocatalytic degradation of sulfamethoxazole in aqueous suspension of TiO_2 . *Appl Catal B* 74:233–241
- Abellan MN, Gimenez J, Esplugas S (2009) Photocatalytic degradation of antibiotics: the case of sulfamethoxazole and trimethoprim. *Catal Today* 144:131–136
- Ahmedchekkat F, Medjram MS, China M, Al-Bsoul AMA (2011) Sono photocatalytic degradation of Rhodamine B using a novel reactor geometry: effect of operating conditions. *Chem Eng J* 178:244–251
- Ajmal A, Majeed I, Malik RN, Idriss H, Nadeem MA (2014) Principles and mechanisms photocatalytic dye degradation on TiO_2 based photocatalysts: a comparative overview. *RSC Adv* 43:7003–37026
- Bandyopadhyay K, Mayya KS, Vijayamohan K, Sastry M (1997) Spontaneously organized molecular assembly of an aromatic organic disulfide on silver/platinum alloy surfaces: an angle dependent X-ray photoemission investigation. *J Electron Spectrosc Relat Phenom* 87:101–107
- Bao J, Guo S, Gao J, Hu T, Yang L, Liu C, Peng J, Jiang C (2015) Synthesis of $\text{Ag}_2\text{CO}_3/\text{Bi}_2\text{WO}_6$ heterojunctions with enhanced photocatalytic activity and cycling stability. *RSC Adv* 5:97195–97204
- Bazin I, Hassine AIH, Hamouda YH, Mnif W, Bartegi A, Lopez-Ferber M, De Waard M, Gonzalez C (2012) Estrogenic and anti-estrogenic activity of 23 commercial textile dyes. *Ecotoxicol Environ Saf* 85:131–136

- Boobas S, Krishnakumar V, Jayaprakash J, Ranjith R, Vijayan J (2017) Preparation of cerium and sulfur codoped TiO_2 nanoparticles based photocatalytic activity with enhanced visible light. *J Photochem Photobiol A* 349:91–99
- Chatterjee D, Dasgupta S (2005) Visible light induced photocatalytic degradation of organic pollutants. *J Photochem Photobiol C* 6:186–205
- Chatzitakis A, Berberidou C, Paspaltsis I, Kyriakou G, Sklaviadis T, Poullos I (2008) Photocatalytic degradation and drug activity reduction of chloramphenicol. *Water Res* 42:386–394
- Chauhan R, Kumar A, Chaudhary RP (2014) Photocatalytic degradation of methylene blue with Cu doped ZnS nanoparticles. *J Lumin* 145:6–12
- Chen X (2002) Preparation and property of TiO_2 nanoparticle dispersed polyvinyl alcohol composite materials. *J Mater Sci Lett* 21:1637–1639
- Chen X, Mao SS (2007) Titanium dioxide nanomaterials: synthesis, properties, modifications, and applications. *Chem Rev* 107:2891–2959
- Cheng H, Lv XJ, Cao S, Zhao ZY, Chen Y, Fu WF (2016) Robustly photogenerating H_2 in water using FeP/CdS catalyst under solar irradiation. *Sci Rep* 6:19846
- Dong S, Feng J, Li Y, Hu L, Liu M, Wang Y, Pi Y, Sun J, Sun J (2014a) Shape-controlled synthesis of BiVO_4 hierarchical structures with unique natural-sunlight-driven photocatalytic activity. *Appl Catal B* 152:413–424
- Dong S, Sun J, Li Y, Yu C, Li Y, Sun J (2014b) ZnSnO_3 hollow nanospheres/reduced graphene oxide nanocomposites as high-performance photocatalysts for degradation of metronidazole. *Appl Catal B* 144:386–393
- Dumrongrojthanath P, Thongtem T, Phuruangrat A, Thongtem S (2013) Hydrothermal synthesis of Bi_2WO_6 hierarchical flowers with their photonic and photocatalytic properties. *Superlattices Microstruct* 54:71–77
- Farzadkia M, Esrafil A, Baghapour MA, Shahamat YD, Okhovat N (2014) Degradation of metronidazole in aqueous solution by nano-ZnO/UV photocatalytic process. *Desalination Water Treat* 52:4947–4952
- Fu H, Pan C, Yao W, Zhu Y (2005) Visible-light-induced degradation of rhodamine B by nanosized Bi_2WO_6 . *J Phys Chem C* 109:22432–22439
- Garcia-Perez UM, Sepulveda-Guzman S, Martinez-De La Cruz A (2012) Nanostructured BiVO_4 photocatalysts synthesized via a polymer-assisted coprecipitation method and their photocatalytic properties under visible-light irradiation. *Solid State Sci* 14:293–298
- Gu W, Liao LS, Cai SD, Zhou DY, Jin ZM, Shi XB, Lei YL (2012) Adhesive modification of indium-tin-oxide surface for template attachment for deposition of highly ordered nanostructure arrays. *Appl Surf Sci* 258:8139–8145
- Guo Y, Zhang G, Gan H, Zhang Y (2012a) Micro/nano-structured $\text{CaWO}_4/\text{Bi}_2\text{WO}_6$ composite: synthesis, characterization and photocatalytic properties for degradation of organic contaminants. *Dalton Trans* 41:12697–12703
- Guo Y, Zhang G, Gan H (2012b) Synthesis, characterization and visible light photocatalytic properties of $\text{Bi}_2\text{WO}_6/\text{rectorite}$ composites. *J Colloid Interface Sci* 369:323–329
- Guo Y, Zhang G, Liu J, Zhang Y (2013) Hierarchically structured $\alpha\text{-Fe}_2\text{O}_3/\text{Bi}_2\text{WO}_6$ composite for photocatalytic degradation of organic contaminants under visible light irradiation. *RSC Adv* 3:2963–2970
- Guo H, Guo Y, Liu L, Li T, Wang W, Chen W, Chen J (2014) Designed hierarchical synthesis of ring-shaped $\text{Bi}_2\text{WO}_6@/\text{CeO}_2$ hybrid nanoparticle aggregates for photocatalytic detoxification of cyanide. *Green Chem* 16:2539–2545

- Guo N, Cao Y, Rong Y, Jia D (2016) Green synthesis of BiOBr modified $\text{Bi}_2\text{O}_2\text{CO}_3$ nanocomposites with enhanced visible-responsive photocatalytic properties. *RSC Adv* 6:106046–106053
- He D, Wang L, Li H, Yan T, Wang D, Xie T (2011) Self-assembled 3D hierarchical clew-like Bi_2WO_6 microspheres: synthesis, photo-induced charges transfer properties, and photocatalytic activities. *CrystEngComm* 13:4053–4059
- Hemalatha KS, Rukmani K (2016) Synthesis, characterization and optical properties of polyvinyl alcohol–cerium oxide nanocomposite films. *RSC Adv* 6:74354–74366
- Jing D, Guo L (2007) Efficient hydrogen production by a composite CdS/mesoporous zirconium titanium phosphate photocatalyst under visible light. *J Phys Chem C* 111:13437–13441
- Jung G, Kim HI (2014) Synthesis and photocatalytic performance of PVA/TiO₂/graphene MWCNT nanocomposites for dye removal. *J Appl Polym Sci* 131:40715
- Kandi D, Martha S, Thirumurugan A, Parida KM (2017) Modification of BiOI microplates with CdS QDs for enhancing stability, optical property, electronic behavior toward Rhodamine B decolorization, and photocatalytic hydrogen evolution. *J Phys Chem C* 121:4834–4849
- Kansal SK, Kundu P, Sood S, Lamba R, Umar A, Mehta SK (2014) Photocatalytic degradation of the antibiotic levofloxacin using highly crystalline TiO₂ nanoparticles. *New J Chem* 38:3220–3226
- Krishnakumar V, Shanmugam G (2012) Structural, optical and dielectric properties of PbS PVA-PEG nanocomposite film. *Sci Adv Mater* 4:1247
- Krishnakumar V, Ranjith R, Jayaprakash J, Boobas S, Venkatesan J (2017) Enhancement of photocatalytic degradation of methylene blue under visible light using transparent Mg-doped CdS–PVA nanocomposite films. *J Mater Sci Mater Electron* 28:13990–13999
- Kudo A, Miseki Y (2009) Heterogeneous photocatalyst materials for water splitting. *Chem Soc Rev* 38:253–278
- Kumar S, Ojha AK (2016) In-situ synthesis of reduced graphene oxide decorated with highly dispersed ferromagnetic CdS nanoparticles for enhanced photocatalytic activity under UV irradiation. *Mater Chem Phys* 171:126–136
- Kummerer K (2009) Antibiotics in the aquatic environment—a review—part I. *Chemosphere* 75:417–434
- Kundu J, Khilari S, Pradhan D (2017) Shape-dependent photocatalytic activity of hydrothermally synthesized cadmium sulfide nanostructures. *ACS Appl Mater Interfaces* 9:9669–9680
- Li W, Li M, Xie S, Zhai T, Yu M, Liang C, Ouyang X, Lu X, Li H, Tong Y (2013) Improving the photoelectron chemical and photocatalytic performance of CdO nanorods with CdS decoration. *CrystEngComm* 15:4212–4216
- Li Y, Li YL, Sa B, Ahuja R (2017) Review of two-dimensional materials for photocatalytic water splitting from a theoretical perspective. *Catal Sci Technol* 7:545–559
- Liu J, Zhang G, Jimmy CY, Guo Y (2013) In situ synthesis of Zn₂GeO₄ hollow spheres and their enhanced photocatalytic activity for the degradation of antibiotic metronidazole. *Dalton Trans* 42:5092–5099
- Liu X, Chen Q, Lv L, Feng X, Meng X (2015a) Preparation of transparent PVA/TiO₂ nanocomposite films with enhanced visible-light photocatalytic activity. *Catal Commun* 58:30–33
- Liu CM, Liu JW, Zhang GY, Zhang JB, Wu QS, Xu YY, Sun YQ (2015b) Facile room temperature precipitation strategy for Ag₂O/Bi₂WO₆ heterojunction with high simulated sunlight photocatalytic performance via bi-directed electron migration mechanism. *RSC Adv* 5:32333–32342
- Liu L, Qi Y, Lu J, Lin S, An W, Hu J, Liang Y, Cui W (2015c) Dramatic activity of a Bi₂WO₆@gC₃N₄ photocatalyst with a core@ shell structure. *RSC Adv* 5:99339–99346
- Luo M, Lu P, Yao W, Huang C, Xu Q, Wu Q, Kuwahara Y, Yamashita H (2016) Shape and composition effects on photocatalytic hydrogen production for Pt–Pd alloy cocatalysts. *ACS Appl Mater Interfaces* 8:20667–20674
- Mallakpour S, Vahabi M (2015) Preparation of poly(vinyl alcohol) nanocomposite films reinforced with poly(amide–imide)/CuO having *N*-trimellitylimido-L-valine linkages for the improvement of mechanical and thermal properties. *Polym Plast Technol Eng* 54:1625–1633
- Mirhoseini F, Salabat A (2015) Ionic liquid based microemulsion method for the fabrication of poly (methyl methacrylate)-TiO₂ nanocomposite as a highly efficient visible light photocatalyst. *RSC Adv* 5:12536–12545
- Moon YE, Jung G, Yun J, Kim HI (2013) Poly(vinyl alcohol)/poly(acrylic acid)/TiO₂/graphene oxide nanocomposite hydrogels for pH-sensitive photocatalytic degradation of organic pollutants. *Mater Sci Eng B* 178:1097–1103
- Ni ZM, Xia SJ, Wang LG, Xing FF, Pan GX (2007) Treatment of methyl orange by calcined layered double hydroxides in aqueous solution: adsorption property and kinetic studies. *J Colloid Interface Sci* 316:284–291
- Priyadharsan A, Vasanthakumar V, Karthikeyan S, Raj V, Shanavas S, Anbarasan PM (2017) Multi-functional properties of ternary CeO₂/SnO₂/rGO nanocomposites: visible light driven photocatalyst and heavy metal removal. *J Photochem Photobiol A Chem* 346:32–35
- Rao JK, Raizada A, Ganguly D, Mankad MM, Satyanarayana SV, Madhu GM (2015) Investigation of structural and electrical properties of novel CuO–PVA nanocomposite films. *J Mater Sci* 50:7064–7074
- Ren F, Zhang J, Wang Y (2015) Enhanced photocatalytic activities of Bi₂WO₆ by introducing Zn to replace Bi lattice sites: a first-principles study. *RSC Adv* 5:29058–29065
- Safari GH, Hoseini M, Seyedsalehi M, Kamani H, Jaafari J, Mahvi AH (2015) Photocatalytic degradation of tetracycline using nanosized titanium dioxide in aqueous solution. *Environ Sci Technol* 12:603–616
- Saison T, Chemin N, Chaneac C, Durupthy O, Ruaux V, Mariey L, Mauge F, Beaunier P, Jolivet JP (2011) Bi₂O₃, BiVO₄, and Bi₂WO₆: impact of surface properties on photocatalytic activity under visible light. *J Phys Chem C* 115:5657–5666
- Saison T, Gras P, Chemin N, Chaneac C, Durupthy O, Brezova V, Colbeau-Justin C, Jolivet JP (2013) New insights into Bi₂WO₆ properties as a visible-light photocatalyst. *J Phys Chem C* 117:22656–22666
- Sarkar AK, Saha A, Tarafder A, Panda AB, Pal S (2016) Efficient removal of toxic dyes via simultaneous adsorption and solar light driven photodegradation using recyclable functionalized amylopectin–TiO₂–Au nanocomposite. *ACS Sustain Chem Eng* 4:1679–1688
- Shanavas S, Priyadharsan A, Ramesh R, Anbarasan PM (2017a) Optimization and detailed stability study on Pb doped ceria nano cubes for enhanced photodegradation of several anionic and cationic organic pollutants. *Arab J Chem*. <https://doi.org/10.1016/j.arabjc.2017.11.001>
- Shanavas S, Priyadharsan A, Vasanthakumar V, Arunkumar A, Anbarasan PM, Bharathkumar S (2017b) Mechanistic investigation of visible light driven novel La₂CuO₄/CeO₂/rGO ternary hybrid nanocomposites for enhanced photocatalytic performance and antibacterial activity. *J Photochem Photobiol A* 340:96–108
- Shangguan W, Yoshida A (2002) Photocatalytic hydrogen evolution from water on nanocomposites incorporating cadmium sulfide into the interlayer. *J Phys Chem B* 106:12227–12230
- Shen S, Guo L (2006) Structural, textural and photocatalytic properties of quantum-sized In₂S₃-sensitized Ti-MCM-41 prepared by ion-exchange and sulfidation methods. *J Solid State Chem* 179:2629–2635

- Silva LA, Ryu SY, Choi J, Choi W, Hoffmann MR (2008) Photocatalytic hydrogen production with visible light over Pt-interlinked hybrid composites of cubic-phase and hexagonal-phase CdS. *J Phys Chem C* 112:12069–12073
- Tang J, Zou Z, Ye J (2007) Efficient photocatalysis on BaBiO₃ driven by visible light. *J Phys Chem C* 111:12779–12785
- Tang R, Su H, Duan S, Sun Y, Li L, Zhang X, Zeng S, Sun D (2015) Enhanced visible light driven photocatalytic performances using Bi₂WO₆/MS (M = Cd, Zn) heterostructures: facile synthesis and photocatalytic mechanisms. *RSC Adv* 5:41949–41960
- Tian Y, Fu J, Chang B, Xi F, Dong X (2012) Synthesis of mesoporous CdS/titania composites with visible light photocatalytic activities. *Mater Lett* 81:95–98
- Wang Y, Deng K, Zhang L (2011) Visible light photocatalysis of BiOI and its photocatalytic activity enhancement by in situ ionic liquid modification. *J Phys Chem C* 115:14300–14308
- Wang C, Wang L, Jin J, Liu J, Li Y, Wu M, Chen L, Wang B, Yang X, Su BL (2016a) Probing effective photocorrosion inhibition and highly improved photocatalytic hydrogen production on monodisperse PANI@CdS core-shell nanospheres. *Appl Catal B* 188:351–359
- Wang Y, Wu Y, Qin Y, Rao J, Chen G, Lv C, Liu B (2016b) The synthesis of elegant hierarchical CdS via a facile hydrothermal method assisted by inorganic salt, with photo corrosion inhibition. *CrystEngComm* 18:7523–7529
- Wang J, Tang L, Zeng G, Liu Y, Zhou Y, Deng Y, Wang J, Peng B (2017) Plasmonic Bi metal deposition and g-C₃N₄ coating on Bi₂WO₆ microspheres for efficient visible-light photocatalysis. *ACS Sustain Chem Eng* 5:1062–1072
- Wei YT, Zheng YM, Chen JP (2011) Enhanced adsorption of arsenate onto a natural polymer based sorbent by surface atom transfer radical polymerization. *J Colloid Interface Sci* 356:234–239
- Wei W, Xie J, Lu X, Osei PB, Yan Z, Meng S, Cui H (2014) CTAB-assisted synthesis and characterization of Bi₂WO₆ photocatalysts grown from WO₃·0.33 H₂O nanoplate precursors. *Monatshefte für Chemie Chem Mon* 145:47–59
- Wong YC, Szeto YS, Cheung W, McKay G (2004) Adsorption of acid dyes on chitosan equilibrium isotherm analyses. *Process Biochem* 39:695–704
- Xiao X, Wei J, Yang Y, Xiong R, Pan C, Shi J (2016) Photoreactivity and mechanism of g-C₃N₄ and Ag co-modified Bi₂WO₆ microsphere under visible light irradiation. *ACS Sustain Chem Eng* 4:3017–3023
- Yu H, Huang X, Wang P, Yu J (2016) Enhanced photoinduced-stability and photocatalytic activity of CdS by dual amorphous cocatalysts: synergistic effect of Ti(IV)-hole cocatalyst and Ni (II)-electron cocatalyst. *J Phys Chem C* 120:3722–3730
- Zeng C, Hu Y, Huang H (2017) BiOBr_{0.75}I_{0.25}/BiOIO₃ as a novel heterojunctional photocatalyst with superior visible-light-driven photocatalytic activity in removing diverse industrial pollutants. *ACS Sustain Chem Eng* 5:3897–3905
- Zhang KL, Liu CM, Huang FQ, Zheng C, Wang WD (2006) Study of the electronic structure and photocatalytic activity of the BiOI photocatalyst. *Appl Catal B Environ* 68:125–129
- Zhang H, Chen X, Li Z, Kou J, Yu T, Zou Z (2007) Preparation of sensitized ZnS and its photocatalytic activity under visible light irradiation. *J Phys D Appl Phys* 40:6846
- Zhang LW, Wang YJ, Cheng HY, Yao WQ, Zhu YF (2009) Synthesis of porous Bi₂WO₆ thin films as efficient visible-light-active photocatalysts. *Adv Mater* 21:1286–1290
- Zhang L, Tian W, Chen Y, Chen J, Teng H, Zhou J, Shi J, Sun Y (2016) Light-driven removal of rhodamine B over SrTiO₃ modified Bi₂WO₆ composites. *RSC Adv* 6:83471–83481
- Zhao C, Pelaez M, Duan X, Deng H, O’Shea K, Fatta-Kassinos D, Dionysiou DD (2013) Role of pH on photolytic and photocatalytic degradation of antibiotic oxytetracycline in aqueous solution under visible/solar light: kinetics and mechanism studies. *Appl Catal B* 134:83–92
- Zheng L, Liu X (2007) Solution-phase synthesis of CuO hierarchical nanosheets at near-neutral pH and near-room temperature. *Mater Lett* 61:2222–2226
- Zhou C, Yan J, Chen B, Li P, Dong X, Xi F, Liu J (2016) Synthesis and application of ternary photocatalyst with a gradient band structure from two-dimensional nanosheets as precursors. *RSC Adv* 6:108955–108963
- Zhu Z, Zhang L, Li J, Du J, Zhang Y, Zhou J (2013) Synthesis and photocatalytic behavior of BiVO₄ with decahedral structure. *Ceram Int* 39:7461–7465
- Zhuo Y, Huang J, Cao L, Ouyang H, Wu J (2013) Photocatalytic activity of snow-like Bi₂WO₆ microcrystalline for decomposition of Rhodamine B under natural sunlight irradiation. *Mater Lett* 90:107–110
- Zou L, Wang H, Wang X (2016) High efficient photodegradation and photocatalytic hydrogen production of CdS/BiVO₄ heterostructure through Z-scheme process. *ACS Sustain Chem Eng* 5:303–309

Publisher’s Note Springer Nature remains neutral with regard to jurisdictional claims in published maps and institutional affiliations.